Article

The Mesozoic terminated in boreal spring

Melanie A. D. During[1,2 ✉], Jan Smit[1], Dennis F. A. E. Voeten[2,3], Camille Berruyer[3], Paul Tafforeau[3], Sophie Sanchez[2,3], Koen H. W. Stein[4,5], Suzan J. A. Verdegaal-Warmerdam[1] & Jeroen H. J. L. van der Lubbe[1,6]

The Cretaceous–Palaeogene mass extinction around 66 million years ago was triggered by the Chicxulub asteroid impact on the present-day Yucatán Peninsula[1,2]. This event caused the highly selective extinction that eliminated about 76% of species[3,4], including all non-avian dinosaurs, pterosaurs, ammonites, rudists and most marine reptiles. The timing of the impact and its aftermath have been studied mainly on millennial timescales, leaving the season of the impact unconstrained. Here, by studying fishes that died on the day the Mesozoic era ended, we demonstrate that the impact that caused the Cretaceous–Palaeogene mass extinction took place during boreal spring. Osteohistology together with stable isotope records of exceptionally preserved perichondral and dermal bones in acipenseriform fishes from the Tanis impact-induced seiche deposits[5] reveal annual cyclicity across the final years of the Cretaceous period. Annual life cycles, including seasonal timing and duration of reproduction, feeding, hibernation and aestivation, vary strongly across latest Cretaceous biotic clades. We postulate that the timing of the Chicxulub impact in boreal spring and austral autumn was a major influence on selective biotic survival across the Cretaceous–Palaeogene boundary.

The Cretaceous-Palaeogene (K–Pg) mass extinction event affected biodiversity with high but poorly understood taxonomic selectivity. Among archosaurs, for example, all pterosaurs and non-avian dinosaurs succumbed in the K–Pg mass extinction, while crocodilians and birds survived into the Palaeogene period[3,4]. Direct consequences of the impact, including impact glass fallout, large-scale forest fires and tsunamis, are geologically documented more than 3,500 km from the Chicxulub impact crater[5–8]. Although direct effects of the impact devastated a vast geographical area, the global mass extinction probably unfolded during its aftermath, which involved rapid climatic deterioration estimated to have lasted up to several thousands of years[9–11]. Whether seasonal timing of the onset of these marked changes affected the selectivity of the K–Pg extinction could not yet be established owing to the lack of suitable records.

The Tanis event deposit in North Dakota (USA) is an exceptional seiche deposit preserving a rich thanatocoenosis (that is, a mass death assemblage) of latest Cretaceous biota at the top of the Hell Creek Formation. The majority of macrofossils encountered at the Tanis locality represent direct casualties of the K–Pg bolide impact that were buried within the impact-induced seiche deposit[5]. Tens of minutes after the impact, the seiche agitated large volumes of water and soil in the estuary of the Tanis river[5]. As the seiche proceeded upstream, it advected bones, teeth, bivalves, ammonites, benthic foraminifera (Extended Data Fig. 1a–c) and plant matter in the suspended load while impact spherules rained down from the sky[5]. Within the thanatocoenotic accumulation, abundant acipenseriforms—sturgeons and paddlefishes—became oriented along the seiche flow directions and buried alive with numerous impact spherules in their gills[5] (Fig. 1, Extended Data Fig. 2a, b).

During the Maastrichtian (that is, the last age of the Cretaceous), the climate of present-day North Dakota involved four seasons that were documented in tree-ring records recovered from other Upper Cretaceous sites in the Hell Creek Formation[12,13]. Tanis was located at approximately 50° N during the latest Cretaceous and experienced distinct seasonality in rainfall and temperature[14]. Regional air temperatures were reconstructed to range from 4–6 °C in winter up to an average of about 19 °C in summer[13,14]. To uncover the season of the K–Pg bolide impact, we analysed osteohistological records of acipenseriform bone apposition in three paddlefish dentaries and three sturgeon pectoral fin spines that were excavated at the Tanis site in 2017 (Extended Data Fig. 1d–j). These skeletal elements preserve unaltered growth records from embryonic development up to death, making them highly suitable for life history reconstructions[15,16].

Growth records of end-Cretaceous fishes

To trace appositional growth and pinpoint the season in which bone apposition terminated, we first assessed the preservation of bone growth patterns across the studied specimens. We prepared dermal bone slices of six acipenseriform specimens as microscopic slides and subjected these to osteohistological assessment, during which lines of arrested growth (LAGs) were easily recognized (Fig. 2). To corroborate the annual nature of the LAGs using virtual high-resolution osteohistology[17,18], three-dimensional (3D) volumes were produced with propagation phase-contrast synchrotron radiation micro-computed tomography[19] on beamline BM05 of the European Synchrotron Radiation Facility, France. The 3D nature of the synchrotron data enables

[1]Department of Earth Sciences, Faculty of Science, Vrije Universiteit Amsterdam, Amsterdam, the Netherlands. [2]Subdepartment of Evolution and Development, Department of Organismal Biology, Evolutionary Biology Centre, Uppsala University, Uppsala, Sweden. [3]European Synchrotron Radiation Facility, Grenoble, France. [4]Royal Belgian Institute of Natural Sciences, Directorate 'Earth and History of Life', Brussels, Belgium. [5]Earth System Science—AMGC, Vrije Universiteit Brussel, Brussels, Belgium. [6]School of Earth and Environmental Sciences, Cardiff University, Cardiff, UK. ✉e-mail: melanie.during@ebc.uu.se
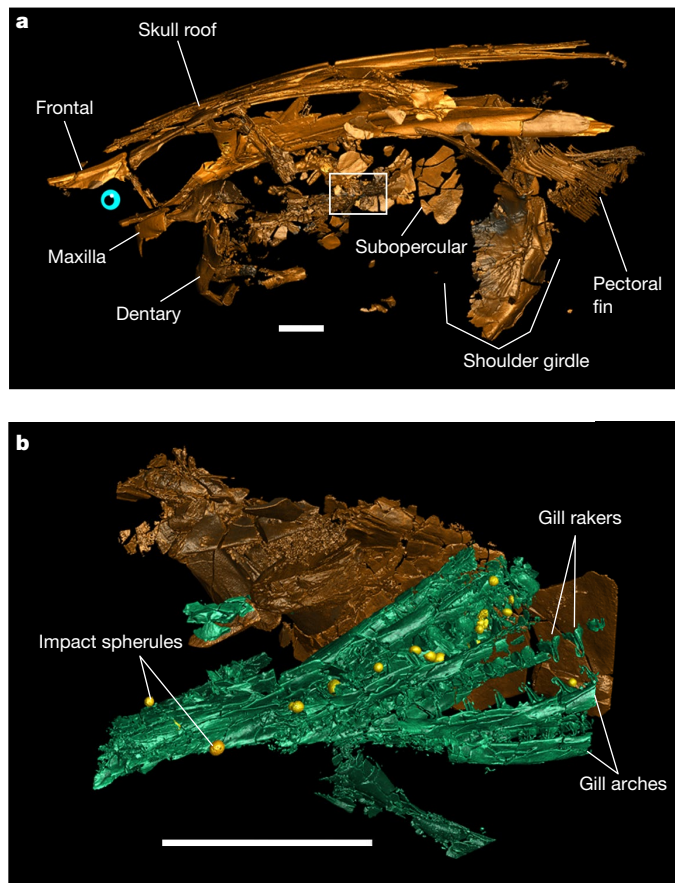
Fig. 2 | Osteohistological thin sections of five acipenseriform fishes. **a**–**e**, Thin sections in transmitted light of VUA.GG.2017.MDX-3 (**a**), VUA. GG.2017.X-2743M (**b**), VUA.GG.2017.X-2744M (**c**), VUA.GG.2017.X-2733A (**d**) and VUA.GG.2017.X-2733B (**e**), showing congruent pacing of bone apposition during the final years of life, terminating in spring. Red arrows indicate LAGs. Scale bars, 0.5 mm.

Fig. 1 | Reconstruction of a paddlefish with impact spherules in the gill rakers. a, Three-dimensional rendering of paddlefish FAU.DGS.ND.161.4559.T in left lateral view with the location of a higher-resolution scan (depicted in **b**) indicated (white outline). **b**, Three-dimensional rendering of the subopercular and gills in **a** with trapped impact spherules (yellow). Scale bars, 2 cm. Two-dimensional tomographic data and fully annotated three-dimensional renderings are provided in Extended Data Fig. 2. A three-dimensional animated rendering of FAU.DGS.ND.161.4559.T is provided as Supplementary Video 1.

optimal projection of the bone deposition pattern across multiple cross-sectional planes and resolved the exact relationship between seasonality and cyclical bone apposition in superb detail[20]. In addition, virtual osteohistology allowed us to visualize the seasonal fluctuations of osteocyte lacunar density and volume, which are poorly expressed in the physical 2D thin sections[18] (Fig. 3c, d) . The osteohistological data (Figs. 2, 3, Extended Data Figs. 3–6) were complemented with an incremental carbon isotope record extracted from one of the paddlefish dentaries (VUA.GG.2017.X-2724).

The tomographic data show that impact spherules associated with the paddlefish skeleton are present exclusively in its gill rakers[5] and are absent elsewhere in the preserved specimen (Fig. 1). The absence of impact spherules outside the gill rakers demonstrates that spherules were filtered out of the surrounding waters but had not yet proceeded into the oral cavity or further down the digestive tract, and had not impacted the fish carcases during perimortem exposure. Impact spherule accumulation in the gill rakers and the arrival of the seiche waves must therefore have occurred simultaneously[5], which implies that the acipenseriforms were alive and foraging during the bolide impact and the last minutes of the Cretaceous.

Well-conserved bone growth archives

The degree of preservation of the sampled acipenseriform bones was assessed using micro-X-ray fluorescence (Methods, Extended
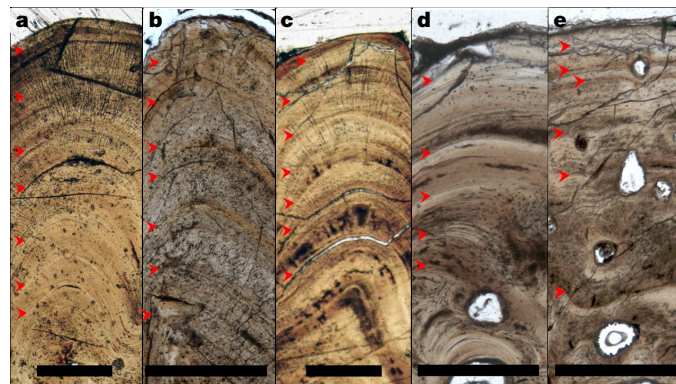
Data Figs. 7–9), which would reveal potential taphonomic elemental exchange that may have affected the primary stable isotope composition. The micro-X-ray fluorescence maps show that Fe and Mn oxides are present in the bone vascular canals and surrounding sediments (Extended Data Fig. 8), but have not invaded the bone apatite ($Ca_5(PO_4, CO_3)_3(OH,F,Cl)$). Detrital components, characterized by high concentrations of K and Si, remain restricted to the sediment matrix (Extended Data Fig. 8f–j). The bone apatite conserves a highly homogeneous distribution of P and Ca (Extended Data Fig. 9), which corroborates the unaltered preservation of these apatitic tissues. Skeletal remains of the paddlefishes and sturgeons thus experienced negligible diagenetic alteration, probably as a consequence of rapid burial and possibly aided by early Mn and Fe oxide seam formation[21,22]. The exquisite 3D preservation of delicate structures, including non-ossified tissues that originally enveloped the brain (Extended Data Fig. 2c–f), further demonstrates the excellent preservation of the fossils and absence of taphonomic reorganization[23].

Consistent records of a spring death

Paddlefish dentaries form through perichondral ossification around the Meckel's cartilage[24]. Sturgeon pectoral fin spines consist of dermal bone—an intramembranous skeletal tissue that forms in the mesenchyme (mesodermal embryonic tissue)[25]. Unlike endochondral bone, perichondral and dermal bone do not originate through mineralization of cartilaginous precursors[26–28] but grow exclusively through incremental bone matrix apposition by secretion of a row of osteoblasts[24,26–28]. The thickness of one annual growth mark cumulatively spans a thick (favourable) growth zone, a thinner (slowly deposited) annulus and, ultimately, a LAG[20]. Our microscopic and virtual osteohistological data consistently show that the six fishes perished (that is, stopped growing) while forming a growth zone shortly after a LAG was deposited (Figs. 2, 3, Extended Data Figs. 3–6), which coincides with an early stage of the favourable growth season[20]. The outermost cortices of all six acipenseriform individuals studied here also exhibit increasing osteocyte lacunar densities and sizes towards their periosteal surfaces (Fig. 3c, Extended Data Figs. 5, 6). In all specimens, this density remained lower than the highest densities and average sizes recorded in previous years (Fig. 3c, Extended Data Figs. 3–6, 10b). As osteocyte lacunar density and size patterns were consistently cyclical across the preceding years during which they peaked at the climaxes of the growth seasons, the last recorded growth season had thus not yet climaxed at the time of death (Figs. 2, 3, Extended Data Figs. 3–6, 10b).
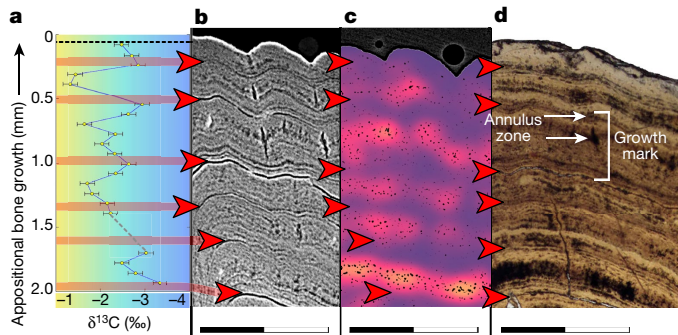
Fig. 3 | Carbon isotope record alongside the incremental growth profiles across the dentary of paddlefish VUA.GG.2017.X-2724. a, δ expressed as ‰ on the Vienna Pee Dee Belemnite (VPDB) reference scale. The colour gradient highlights the theoretical range between maximum values during seasonal (summer) trophic increase of ^{13}C (yellow) and minimum values during trophic decrease of ^{13}C (winter) (blue). **b**, Virtual thick section (average-value projection with 0.1-mm depth) showing growth zones during the favourable growth seasons and annuli and LAGs outside the favourable growth seasons. **c**, Cell density map[51] of a virtual thick section (minimum-value projection with 0.2-mm depth) showing fluctuating osteocyte lacunar densities and sizes, with higher densities and largest sizes recorded during the favourable growth seasons (orange) and lower densities and smaller sizes outside the favourable growth seasons (purple). A comparative image of a larger section of bone with scale is provided in Extended Data Fig. 6. **d**, Microscopic thin section in transmitted light showing LAGs (red arrows) and a single growth mark indicated (bracket) spanning the distance between two subsequent LAGs and including a zone and an annulus (Extended Data Fig. 10b). Scanning data visualized in **b** and **c** were obtained approximately 10-mm distal from the physically sectioned thin slice of **d**, which itself was located directly proximal to the thick section sampled for **a**. Scale bars, 1 mm. Corresponding osteohistological data of the other five sampled acipenseriform fishes are presented in Extended Data Figs. 3–5.

The inferred annual growth cycles are independently corroborated by a stable carbon isotope ($\delta^{13}C_{sc}$) archive that recorded several years of seasonal dietary fluctuations in growing bone. Paddlefish VUA.GG.2017.X-2724 also yielded, in addition to this $\delta^{13}C_{sc}$ archive, an oxygen isotope ($\delta^{18}O_{sc}$) record across the final six years of its life (Supplementary Data Table 1, Extended Data Fig. 10a, Methods). The low and constant $\delta^{18}O_{sc}$ values in VUA.GG.2017.X-2724 reflect exclusive inhabitation of freshwater environments by the paddlefishes. This implies that their osteohistological records must have captured seasonal variability rather than, for example, migration between saline and freshwater habitats. Although modern sturgeons are known to have anadromous lifestyles[29,30], this remains to be confirmed for the fossil sturgeons at Tanis, as isotopic data from sturgeon pectoral fin spines could not be secured (Methods, 'Micromill'). Notably, the osteohistological records of all our sturgeons and paddlefishes converge on the same annual growth phase, despite their potential different lifestyles.

Like their modern-day relatives, the latest Maastrichtian paddlefishes of Tanis were filter feeders that presumably consumed copepods and other zooplankton[29–31]. These fishes probably experienced an annual feeding pattern, determined by fluctuating food availability, that peaked between spring and autumn[31]. During maximum productivity, ingested zooplankton enriches the growing skeleton of filter-feeding fishes with ^{13}C relative to ^{12}C[32,33]. Thus, the cyclically elevated $^{13}C/^{12}C$ ratios in paddlefish VUA.GG.2017.X-2724 (Fig. 3a) reflect distinct episodes of high food availability and consumption. Carbon isotope records across the growth record of Paddlefish VUA.GG.2017.X-2724 indicate that peak annual growth rate was not yet attained and the feeding season had thus not yet climaxed—corroborating a boreal spring death.

Implications for selective K–Pg survival

The Chicxulub bolide impact caused a global heat pulse that ignited widespread wildfires[9,34]. After this heat wave, the last boreal spring of the Mesozoic transitioned to a global impact winter[10]. Although a June timing for the K–Pg impact has been suggested on the basis of palaeobotanical indications for anomalous freezing in this region (Wyoming, USA)[35], the palaeobotanical identities, taphonomic inferences and stratigraphic assumptions underlying that conclusion have since all been refuted[36–39]. Moreover, post-impact cooling happened in the first months to decades following the K–Pg impact[10], which renders proxies registering post-impact freezing conditions asynchronous with the impact event itself.

A suite of impact-induced phenomena contributed to the K–Pg extinction on differing timescales[40,41]. In the days to months following the impact, its instantaneous effects, such as intense infrared radiation caused by ejecta reentry[34], resulting wildfires[9,34] and the spread of sulfurous aerosols leading to acid precipitation[42] must have predominantly afflicted the exposed continental environments. Although negotiating these hostile conditions would not have guaranteed survival, an early clade-wide eradication would always have meant immediate extinction[41].

The seasonal timing of the catastrophic end-Cretaceous bolide impact places the event at a particularly sensitive stage for biological life cycles in the Northern Hemisphere. In many taxa, annual reproduction and growth take place during spring. Species with longer incubation times, such as non-avian reptiles, including pterosaurs and most dinosaurs, were arguably more vulnerable to sudden environmental perturbations than other groups[43] (for example, birds). Southern Hemisphere ecosystems, which were struck during austral autumn, appear to have recovered up to twice as fast as Northern Hemisphere communities[44], consistent with a seasonal effect on biotic recovery.

Subterranean sheltering conceivably contributed to the cynodont survival of the Permo-Triassic (PT) crisis[45]. Similarly, large-scale wildfires raging across the Southern Hemisphere[9,34,41] may have been evaded by hibernating mammals that were already sheltered in burrows[34,41] in anticipation of austral winter. Additional modes of seasonal dormancy, torpor and/or aestivation, which are nowadays practised by various mammals[46,47] as well as certain amphibians, birds and crocodilians[48], could have facilitated further underground survival. In the aftermath of the K–Pg event, ecological networks collapsed from the bottom up. Floral necrosis[9] and extinction immediately affected species dependent on primary producers, while some animals capable of exploiting alternative resources—for example, certain birds and mammals[49,50]—persisted.

Conclusions

Seasonal timing of the Chicxulub impact in boreal spring and austral autumn will aid in further calibrating evolutionary models exploring the selectivity of the K–Pg extinction and the asymmetry in extinction and recovery patterns between the two hemispheres. Decoupling short- and long-term effects of the bolide impact on the K–Pg mass extinction will also aid in identifying extinction risks and modes of ecological deterioration caused by the forthcoming global climate change. The uniquely constrained Tanis site[5] offers valuable proxies for reconstructing the environmental, climatological and biological conditions that prevailed locally when the Mesozoic ended.

Online content

Any methods, additional references, Nature Research reporting summaries, source data, extended data, supplementary information, acknowledgements, peer review information; details of author contributions and competing interests; and statements of data and code availability are available at https://doi.org/10.1038/s41586-022-04446-1.

Article

1. Alvarez, L. W., Alvarez, W., Asaro, F. & Michel, H. V. Extraterrestrial cause for the Cretaceous–Tertiary extinction. *Science* **208**, 1095–1108 (1980).
2. Smit, J. & Hertogen, J. An extraterrestrial event at the Cretaceous–Tertiary boundary. *Nature* **285**, 198–200 (1980).
3. Raup, D. M. Biological extinction in earth history. *Science* **231**, 1528–1533 (1986).
4. Schulte, P. et al. The Chicxulub asteroid impact and mass extinction at the Cretaceous–Paleogene boundary. *Science* **327**, 1214–1218 (2010).
5. DePalma, R. A. et al. A seismically induced onshore surge deposit at the KPg boundary, North Dakota. *Proc. Natl Acad. Sci. USA* **116**, 8190–8199 (2019).
6. Smit, J. et al. Tektite-bearing, deep-water clastic unit at the Cretaceous–Tertiary boundary in northeastern Mexico. *Geology* **20**, 99–103 (1992).
7. Alvarez, W. in *The Cretaceous-Tertiary Event and Other Catastrophes in Earth History* (eds Ryder, G. et al.) 141–150 (Geological Society of America, 1996).
8. Smit, J. The global stratigraphy of the Cretaceous–Tertiary boundary impact ejecta. *Annu. Rev. Earth Planet. Sci.* **27**, 75–113 (1999).
9. Morgan, J., Artemieva, N. & Goldin, T. Revisiting wildfires at the K–Pg boundary. *J. Geophys. Res.* **118**, 1508–1520 (2013).
10. Vellekoop, J. et al. Rapid short-term cooling following the Chicxulub impact at the Cretaceous–Paleogene boundary. *Proc. Natl Acad. Sci. USA* **111**, 7537–7541 (2014).
11. Vellekoop, J. et al. Evidence for Cretaceous-Paleogene boundary bolide 'impact winter' conditions from New Jersey, USA. *Geology* **44**, 619–622 (2016).
12. Golovneva, L. B. The Maastrichtian (Late Cretaceous) climate in the northern hemisphere. *J. Geol. Soc. Lond.* **181**, 43–54 (2000).
13. Wolfe, J. A. & Upchurch Jr, G. R. North American nonmarine climates and vegetation during the Late Cretaceous. *Palaeogeogr. Palaeocl.* **61**, 33–77 (1987).
14. Hallam, A. A review of Mesozoic climates. *J. Geol. Soc. London* **142**, 433–445 (1985).
15. Adams, L. A. Age determination and rate of growth in *Polyodon spathula*, by means of the growth rings of the otoliths and dentary bone. *Am. Midl. Nat.* **28**, 617–630 (1942).
16. Bakhshalizadeh, S., Bani, A., Abdolmalaki, S. & Moltschaniwskyj, N. Identifying major events in two sturgeons' life using pectoral fin spine ring structure: exploring the use of a non-destructive method. *Environ. Sci. Pollut. R* **24**, 18554–18562 (2017).
17. Sanchez, S., Ahlberg, P. E., Trinajstic, K. M., Mirone, A. & Tafforeau, P. Three-dimensional synchrotron virtual paleohistology: a new insight into the world of fossil bone microstructures. *Microsc. Microanal.* **18**, 1095–1105 (2012).
18. Davesne, D., Schmitt, A. D., Fernandez, V., Benson, R. B. & Sanchez, S. Three-dimensional characterization of osteocyte volumes at multiple scales, and its relationship with bone biology and genome evolution in ray-finned fishes. *J. Evol. Biol.* **33**, 808–830 (2020).
19. Tafforeau, P., Bentaleb, I., Jaeger, J.-J. & Martin, C. Nature of enamel laminations and mineralization in rhinoceros enamel using histology and X-ray synchrotron microtomography: potential implications for palaeoenvironmental isotopic studies. *Palaeogeogr. Palaeocl.* **246**, 206–227 (2007).
20. Castanet, J. *Bone—Volume 7: Bone Growth* (ed. Hall, B. K.) 245–283 (CRC Press, 1993).
21. Hedges, R. E. Bone diagenesis: an overview of processes. *Archaeometry* **44**, 319–328 (2002).
22. Dumont, M. et al. Synchrotron XRF analyses of element distribution in fossilized sauropod dinosaur bones. *Powder Diffr.* **24**, 130–134 (2009).
23. Pradel, A. et al. Skull and brain of a 300-million-year-old chimaeroid fish revealed by synchrotron holotomography. *Proc. Natl Acad. Sci. USA* **106**, 5224–5228 (2009).
24. Weigele, J. & Franz-Odendaal, T. A. Functional bone histology of zebrafish reveals two types of endochondral ossification, different types of osteoblast clusters and a new bone type. *J. Anat.* **229**, 92–103 (2016).
25. Enlow, D. H. *The Human Face. An Account of the Postnatal Growth and Development of the Craniofacial Skeleton* (Harper and Row, 1968).
26. Grande, L. & Bemis, W. E. Osteology and phylogenetic relationships of fossil and recent paddlefishes (Polyodontidae) with comments on the interrelationships of Acipenseriformes. *J. Vert. Paleo.* **11**, 1–121 (1991).
27. De Ricqlès, A. J., Meunier, F. J., Castanet, J. & Francillon-Vieillot, H. *Bone 3, Bone Matrix and Bone Specific Products* (CRC Press, 1991).
28. Hall, B. K. *Bones and Cartilage: Developmental and Evolutionary Skeletal Biology* (Elsevier, 2005).
29. Bemis, W. E. & Kynard, B. Sturgeon rivers: an introduction to acipenseriform biogeography and life history. *Environ. Biol. Fish* **48**, 167–183 (1997).
30. LeBreton, G. T., Beamish, F. W. H. & McKinley, S. R. (eds) *Sturgeons and paddlefish of North America,* Vol. 27 (Springer, 2004)
31. Blackwell, B. G., Murphy, B. R. & Pitman, V. M. Suitability of food resources and physicochemical parameters in the lower Trinity River, Texas for paddlefish. *J. Freshw. Ecol.* **10**, 163–175 (1995).
32. Fry, B. & Sherr, E. B. $\delta^{13}C$ measurements as indicators of carbon flow in marine and freshwater ecosystems. *Ecol. Stud.* https://doi.org/10.1007/978-1-4612-3498-2_12 (1989).
33. Finlay, J. C. Stable-carbon-isotope ratios of river biota: implications for energy flow in lotic food webs. *Ecology* **82**, 1052–1064 (2001).
34. Robertson, D. S., Lewis, W. M., Sheehan, P. M. & Toon, O. B. K–Pg extinction: reevaluation of the heat-fire hypothesis. *J. Geophys. Res.* **118**, 329–336 (2013).
35. Wolfe, J. A. Palaeobotanical evidence for a June 'impact winter' at the Cretaceous/Tertiary boundary. *Nature* **352**, 420–423 (1991).
36. Nichols, D. J. Plants at the K/T boundary. *Nature* **356**, 295–295 (1992).
37. Hickey, L. J. & McWeeney, L. J. Plants at the K/T boundary. *Nature* **356**, 295–296 (1992).
38. McIver, E. E. Paleobotanical evidence for ecosystem disruption at the Cretaceous–Tertiary boundary from Wood Mountain, Saskatchewan, Canada. *Can. J. Earth Sci.* **36**, 775–789 (1999).
39. Upchurch, G. R., Lomax, B. H. & Beerling, D. J. Paleobotanical evidence for climatic change across the Cretaceous–Tertiary boundary, North America: twenty years after Wolfe and Upchurch. *Cour. Forsch. Senck* **258**, 57 (2007).
40. Kring, D. A. The Chicxulub impact event and its environmental consequences at the Cretaceous–Tertiary boundary. *Palaeogeogr. Palaeocl.* **255**, 4–21 (2007).
41. Robertson, D. S., McKenna, M. C., Toon, O. B., Hope, S. & Lillegraven, J. A. Survival in the first hours of the Cenozoic. *Geol. Soc. Am. Bull.* **116**, 760–768 (2004).
42. D'Hondt, S., Pilson, M. E., Sigurdsson, H., Hanson Jr, A. K. & Carey, S. Surface-water acidification and extinction at the Cretaceous–Tertiary boundary. *Geology* **22**, 983–986 (1994).
43. Erickson, G. M., Zelenitsky, D. K., Kay, D. I. & Norell, M. A. Dinosaur incubation periods directly determined from growth-line counts in embryonic teeth show reptilian-grade development. *Proc. Natl Acad. Sci. USA* **114**, 540–545 (2017).
44. Donovan, M. P., Iglesias, A., Wilf, P., Labandeira, C. C. & Cúneo, N. R. Rapid recovery of Patagonian plant–insect associations after the end-Cretaceous extinction. *Nat. Ecol. Evol.* **1**, 0012 (2016).
45. Fernandez, V. et al. Synchrotron reveals Early Triassic odd couple: injured amphibian and aestivating therapsid share burrow. *PLoS ONE* **8**, e64978 (2013).
46. Nowack, J., Cooper, C. E. & Geiser, F. Cool echidnas survive the fire. *Proc. R. Soc. B* **283**, 20160382 (2016).
47. Lovegrove, B. G., Lobban, K. D. & Levesque, D. L. Mammal survival at the Cretaceous–Paleogene boundary: metabolic homeostasis in prolonged tropical hibernation in tenrecs. *Proc. R. Soc. B* **281**, 20141304 (2014).
48. Withers, P. C. & Cooper, C. in *Encyclopedia of Ecology* (eds Jorgensen, S. E. & Fath, B.) 952–957 (Elsevier, 2008).
49. Field, D. J. et al. Early evolution of modern birds structured by global forest collapse at the end-Cretaceous mass extinction. *Curr. Biol.* **28**, 1825–1831 (2018).
50. Schleuning, M. et al. Ecological networks are more sensitive to plant than to animal extinction under climate change. *Nat. Commun.* **7**, 13965 (2016).
51. Sanchez, S. et al. 3D microstructural architecture of muscle attachments in extant and fossil vertebrates revealed by synchrotron microtomography. *PloS ONE* **8**, e56992 (2013).